International Research Journal of Pure & Applied Chemistry
4(6): 785-796, 2014

SCIENCEDOMAIN *international*
www.sciencedomain.org

Electronic Transport at Low Temperature in Ni/Al/Ni Films

R. Ramanna[1], P. J. Sadashivaiah[1], T. Sankarappa[1*], T. Sujatha[1], J. S. Ashwajeet[1], A. W. Manjunath[1] and Santosh Kori[1]

[1]Department of Physics, Gulbarga University, Gulbarga 585 106, Karnataka, India.

This research work was carried out in collaboration between all authors. Authors RR and PJS conducted experiments, wrote manuscript and performed statistical analysis. Author TS has designed the study, wrote the protocol, supervised the work and corrected all the drafts of the manuscript and author JSA set the experiments and managed analysis. Authors T. Sujatha, AWM and SK have managed the literature searches and proof read the manuscript. All the authors read and approved the final manuscript.

Original Research Article

Received 1st May 2014
Accepted 1st July 2014
Published 20th July 2014

ABSTRACT

A series of sandwiched films in the configuration, Ni(100nm)/Al(t)/Ni(100nm); t = 10nm, 20nm,……, 100nm (labeled as NAN1, NAN2, ……., NAN10) were deposited by thermal and electron beam gun evaporation techniques. The films were deposited onto the glass substrates held at 473K, under high vacuum conditions. The structure, grain size and interplanar distances were probed by X-ray diffraction (XRD). The grains were of few nanometers in dimension and their size decreased with increasing, t. Electrical resistivity in the temperature range from 4.2K to 300K has been measured. The resistivity decreased nonlinearly and continuously with increasing temperature for the films NAN1, NAN3 and NAN7 similar to that of a semiconductor. Mott's small polaron hopping and variable range hopping models due to Mott and Greave have been employed to understand resistivity variation with temperature in these three films. Remaining seven films exhibited metallic to semiconductor (MST) transition. These results are significant as neither of the constituent layers in the present films is semiconducting by nature. The resistivity data of NAN4 and NAN5 films has been analyzed using semi-classical conductivity model of Boltzman which incorporates quantum corrections in to it. The data belonging to the metallic region of the remaining five films has been analyzed using the conventional Matheissen's rule, as these films

**Corresponding author: Email: sankarappa@rediffmail.com;*

produced only small amount of data in the semiconducting region. It is for the first time that the sandwiched films of the present configuration have been investigated for structure and low temperature resistivity and data analyzed thoroughly.

Keywords: Sandwich films; XRD; metal to semiconductor transition; resistivity.

1. INTRODUCTION

Currently there is enormous interest in layered magnetic films that may be due to the fact that layering can be used for tuning the properties or to obtain properties which were not characteristic of their bulk forms. For practical reasons, the present work is restricted to the study of a simple structure consisting of two magnetic layers separated by a layer of nonmagnetic material. Very extensive experimental and theoretical investigations on exchange coupling [1-3] and magneto--optical kerr-effect [4,5] have been reported on some of these kinds of structures. In some studies, chromium (Cr) spacer instead of copper like metal has been used and investigated the effects of interface roughness [6,7], magnetic and electronic structures [8]. An anomalous behavior of low temperature resistivity has been observed in the structure, Co/M/Co (M = Cr or Cr/Ag or Ag/Cr) [9]. The effect of Cu interlayer on grain size and stress has been investigated in sputtered Fe/Cu multilayers [10]. The structural properties were studied for Fe/Cu multilayers as a function of Fe layer thickness [11]. Some of these studies were aimed at optimizing the planar structure of (111) Au/Co/Cu trilayers [12]. The detailed studies of structure, surface morphology and low temperature electrical properties of Ni/Al/Ni sandwiches have not been reported so far. Pure semiconducting behavior has been observed in oxidized Ni films [13] and a sign for metal to semiconductor transition has been noticed in Pb films [14] at low temperature. Metallic behavior of electrical conductivity at low temperature has been detected in Fe/Cu/Fe sandwiched films [15]. In the present article, we report investigations on structural and electrical properties of Ni/Al/Ni films for different Al spacer layer thicknesses. The layer structure of these films are, [Ni(100nm)/Al(t)/Ni(100nm)]; t=10nm, 20nm, 30nm, 40nm, 50nm, 60nm, 70 nm, 80nm, 90nm and 100nm.

2. EXPERIMENTAL

The sandwich films, (Ni/Al/Ni) were prepared using electron beam gun and thermal evaporation techniques at a pressure 7x10-6 mbar (=1.143 Pa) and temperature 473K. The nickel layers were deposited by evaporating the nickel source from a molybdenum crucible using electron beam gun technique, where as aluminum layers were deposited by thermally evaporating the source from a tungsten filament. The thickness of the layers was measured during deposition using quartz crystal thickness monitor. The films were allowed to cool to room temperature in the vacuum chamber over night and were later subjected to XRD studies in Brucker-D8 advance diffractometer with Cu-Kα radiation of wavelength 1.5406 Å. Electrical resistivity was measured by following four point methods in an Oxford Instruments make resistivity setup in the temperature range from 4.2K to 300K.

3. RESULTS AND DISCUSSION

3.1 X-ray Diffraction (XRD) Studies

The complete XRD spectrum for NAN1 film is shown in Fig.1. Similar spectra were recorded for all the films. The spectra consist of single peak revealing dominant (111) texture of the films. A small variation in the peak positions has been observed for different films which lie between 2θ=44.29 and 44.61 [Table.1]. The grain sizes were determined using Scherrer's formula [16], $D=(0.9\lambda)/(B\cos\theta_B)$, where D defines the grain size, B the angular width in terms of 2θ, θ_B the Bragg angle and λ the wavelength of the radiation.

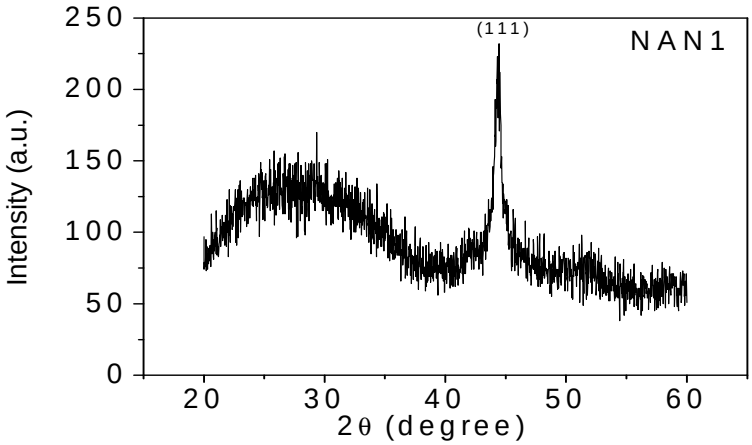

Fig.1. XRD spectra for NAN1 film

The interplanar spacing of the films were calculated using the relation, $d = \lambda/(2 \sin \theta_B)$. The grain sizes were found to be of few nanometers. The interplanar spacing is lying between 2.029 Á and 2.043 Á. The measured peak widths are in the range of 0.638 Á and 0.945 Á.

Table 1. Parameters extracted from XRD spectra for NAN sandwiched films

Film	Thickness of Al, t (nm)	Peak position, 2θ (degrees)	Peak width, Á	Grain size, D (nm)	Interplanar spacing, d (Å)
NAN1	10	44.359	0.754	11.37	2.040
NAN2	20	44.346	0.945	9.077	2.041
NAN3	30	44.294	0.685	12.51	2.043
NAN4	40	44.374	0.756	11.35	2.040
NAN5	50	44.392	0.694	12.37	2.039
NAN6	60	44.516	0.698	12.29	2.033
NAN7	70	44.491	0.690	12.44	2.034
NAN8	80	44.524	0.798	10.76	2.033
NAN9	90	44.573	0.662	12.96	2.031
NAN10	100	44.610	0.638	13.47	2.029

3.2 Electrical Conductivity

The measured temperature variation of resistivity of all the present films revealed the following information.

The films NAN1, NAN3 and NAN7 showed semiconducting behavior. Remaining all the seven films exhibited metal to semiconductor transition (MST).

The present series of films are differing from one another in terms of interfacer layer thickness only. Despite this, the films behaved differently in terms of their electrical resistivity as some of them exhibited semiconducting behavior and some have shown MST transition. The MST transition shown by the present films is similar to ZnO doped systems [17,18]. Indeed, the resistivity measurements have been done twice on the same samples without lifting them from the cryostat. In both the attempts the results were obtained be same. The data was averaged and analyzed. The MST transition temperatures, Tc, are shown in Table 2. The plots of temperature variation of ρ for all the films are depicted in Fig. 2. From the figure, it can be seen that in the entire experimental range of temperature NAN1, NAN3 and NAN7 films behave like a semiconductors. That is, their resisitivity decreases continuously with increasing temperature. NAN4 film exhibited metal to semiconductor transition showing minimum resistivity at a transition temperature, T_c. Transition temperature did not vary systematically with interfacer layer thickness as can be seen in Table.2. NAN5 film produced exactly the same type of ρ versus T spectrum. Whereas NAN10 film along with NAN2, NAN6, NAN8 and NAN9 measured a short tail on the semiconducting side although MST is quite evident in these film also.

Table. 2. The MST transition temperature, T_c, of NAN sandwich films

Films →	**NAN2**	**NAN4**	**NAN5**	**NAN6**	**NAN8**	**NAN9**	**NAN10**
T_C (K) →	41.12	88.24	80.69	13.96	36.53	24.36	21.43

3.2.1 Resistivity variation of NAN1, NAN3 and NAN7 films

Resistivity of NAN1, NAN3 and NAN7 films are in the order of 10-6 Ωm. The room temperature conductivity of these films are in agreement with NiO thin film [19] and higher than that of thick NiO films and Nio nano crystals [20,21]. Resistivity of these three films decreased continuously with increase in temperature resembling semiconductor behavior. The conducitivity data of these films has been analysed using Mott's small polaron hopping and variable range hopping models due to Mott's and Greaves. For higher temperature, Mott's SPH model gave an expression for conductivity as

$$\sigma = (\sigma_0 / T)\exp(-\Delta E / k_B T) \quad (1)$$

Where ΔE is the activation energy and σ0 the pre-exponential factor [22]. The plots of ln (σT) versus (1/T) for these three films are shown in Fig. 3. The least square linear lines were fit to the data for temperatures above θ_D, where θ_D is the Debye's temperature below which the data deviates from linearity. From the slopes, the activation energy, ΔE, was determined and mentioned in Table 3. These activation energy values are smaller than that reported for NiO films and nanocrystals [19-21].

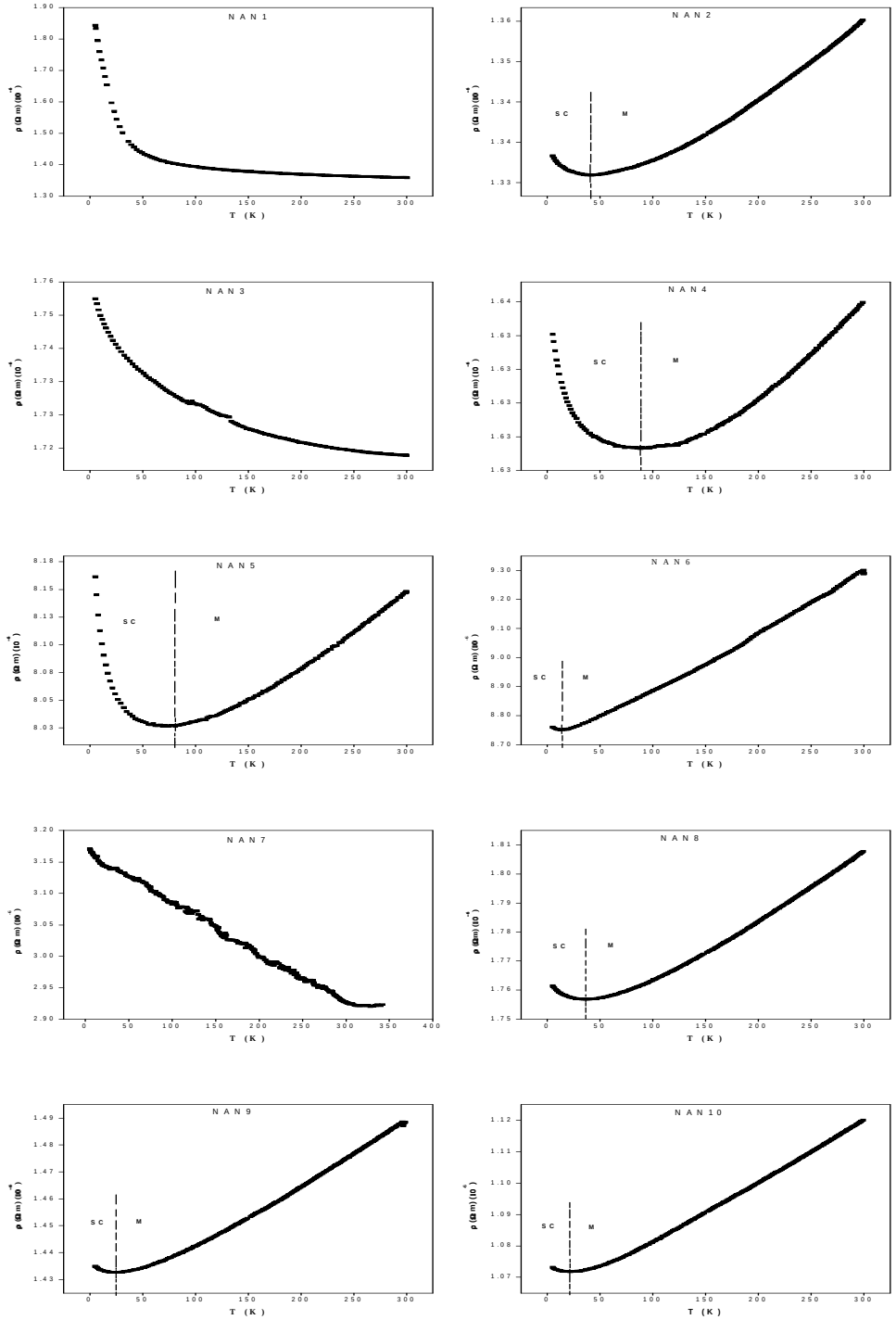

Fig. 2. Temperature variation of resistivity of NAN films. M refers to metallic region and SC refers to semiconducting region

For the data below θ_D, the variable-range hopping (VRH) models due to Mott [23] and Greave [24] have been applied. In Mott's VRH model, the conduction is based on a single optical phonon approach and the conductivity is expressed as,

$$\sigma = A\exp(-T_0/T)^{\frac{1}{4}} \tag{2}$$

Where, $T_0 = 256\,[2\alpha^3/9\pi\, K_B N(E_F)]$ and $A = [e^2/2(8\pi)^{1/2}]\, v_0\,[N(E_F)/\alpha\, K_B T]^{1/2}$

With $N(E_F)$ being the density of states at the Fermi level. The constants A and T_0 are obtained from the ln(σ) versus $T^{-1/4}$ plots as shown in Fig. 4. Only part of the data below θ_D for which the Motts VRH model fit was in good agreement, is only shown in Fig. 4. It is commonly held that much use of the exponent T0 has been made to extract values of $N(E_F)$, given assuming value for α= 10 nm–1 [25,26]. The $N(E_F)$ values obtained are shown in Table 3. These $N(E_F)$ values are much higher than that quoted for NiO nanocrystals [21].

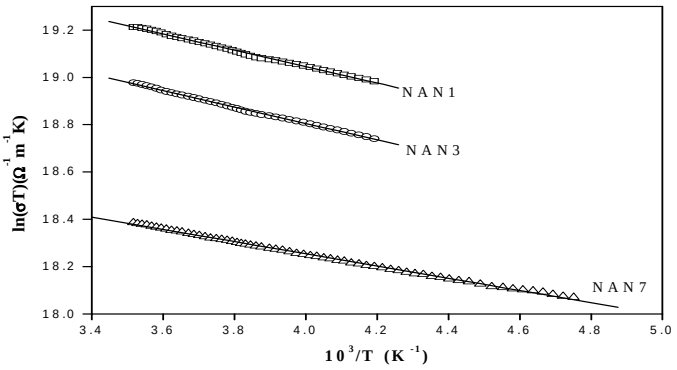

Fig. 3. The plots of ln(σT) versus (1/T) for NAN1, NAN3 and NAN7 films for $T > \theta_D$. Solid lines shown are the linear fits to the data

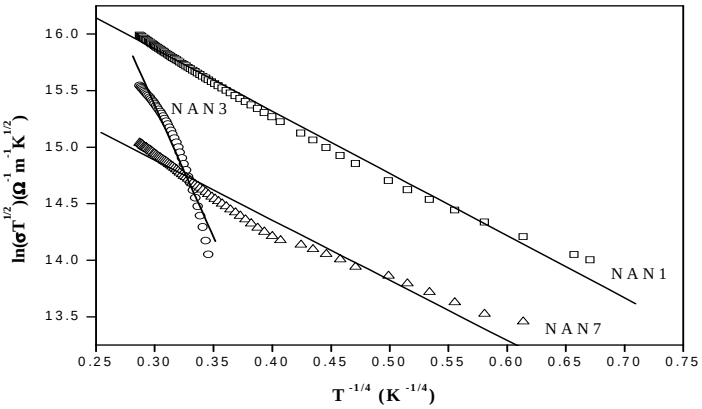

Fig. 4. Plots of ln(σ) versus $T^{-1/4}$ for NAN1, NAN3 and NAN7 films as per Mott's VRH model. Solid lines shown are the linear fits for $T < (\theta_D)$

The data deviated from Mott's VRH has been considered under Greaves VRH model [24]. According to this model, the conductivity is given by

$$\sigma T^{1/2} = B\exp(-T_0 / T)^{1/4} \tag{3}$$

Where, $T_0 = (2.1)^4[\alpha^3 / k_B N(E_F)]$

The Greaves plots of $\ln(\sigma T^{1/2})$ versus $T^{-1/4}$ are shown in Fig. 5. From the fit parameters of B and T_0, the density of states at Fermi level, $N(E_F)$ due to Greaves model were determined and recorded in Table 3. Both the VRH models appeared to fit well with the data in certain range of temperature. However, $N(E_F)$ values deduced from these model fits are high compared to that of the reported values for other thin films. It can therefore be concluded that the conductivity of the present films at very low temperatures cannot be satisfactorily explained using Mott's and Greaves VRH models.

Table 3. Activation energy, ΔE and density of states, $N(E_F)$ determined from Mott's and Greaves model fits

Film	Mott's SPH ΔE (meV)	Mott's VRH $N(E_F)$ ($ev^{-1}cm^{-3}$)	Greaves VRH $N(E_F)$ ($ev^{-1}cm^{-3}$)
NAN1	23.80	2.094X1027	2.446X1022
NAN3	23.29	2.106X1033	5.666X1022
NAN7	23.80	9.480X1029	4.975X1026

Activation energy of all the three films is of the same size approximately. This means that interfacer layer thickness do not affect significantly the activation of conduction process.

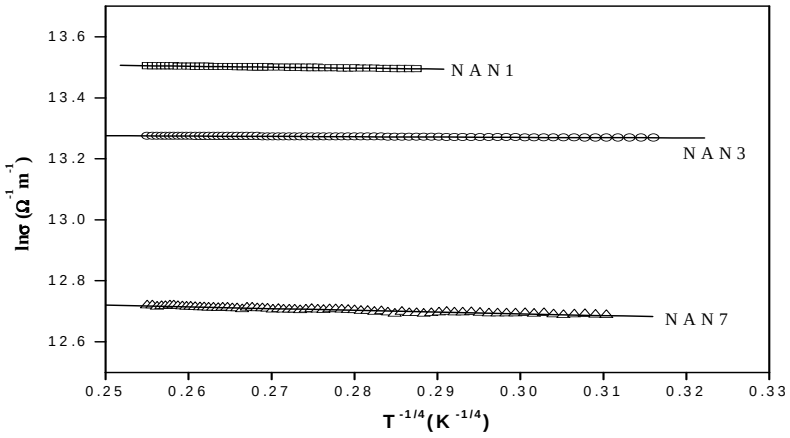

Fig. 5. The plots of $\ln(\sigma T^{1/2})$ versus $T^{-1/4}$ for the films as per Greaves VRH model. Solid lines shown are the liner fits to the data

3.2.2 Resistivity variation of NAN2, NAN4, NAN5, NAN6, NAN8, NAN9 and NAN10 films

The films NAN2, NAN4, NAN5, NAN6, NAN8, NAN9 and NAN10 showed Metal to Semiconductor transition (MST). Of these, NAN4 and NAN5 films have exhibited extended tails on either sides of the transition temperature. Hence, these films have been considered separately for analysis. Other films which have got only short tails on semiconducting side have been considered for analysis under one group. Resistance varied linearly with temperature for NAN2, NAN6, NAN8, NAN9 and NAN10 films for temperature above 150K (Fig. 6). Temperature coefficient of resistance TCR=(dρ/dT)/ρ_{300K} has been determined and recorded in Table. 4. TCR values are positive and are of the order 10^{-4} K^{-1}. TCR value of NAN6 is found to be higher than NAN2, NAN8, NAN9 and NAN10 films.

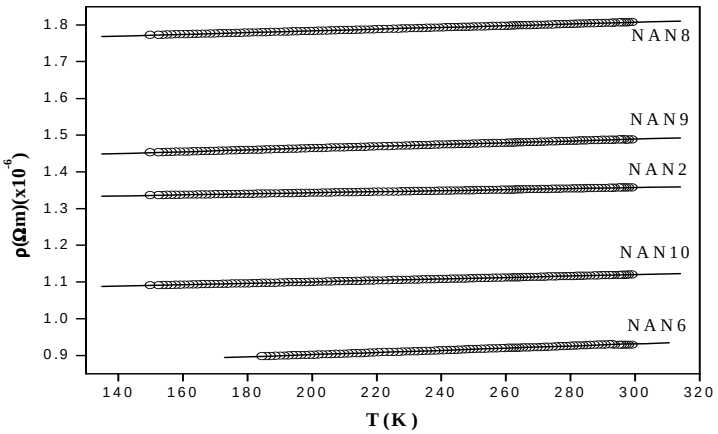

Fig. 6. Plots of ρ vs T for NAN2, NAN6, NAN8, NAN9 and NAN10 films for T > 150K. The lines drawn are the linear fits to the data as per Matheissen's rule

Table 4. Temperature coefficient of resistance, TCR of NAN2, NAN6, NAN8, NAN9 and NAN10 films

Films →	NAN2	NAN6	NAN8	NAN9	NAN10
TCR x $10^{-4}(K)^{-1}$ →	1.050	2.323	1.307	1.644	1.755

Further, linear variation of resisitivity with temperature above 150K is in agreement with Matheissen's rule. According to Matheissen's rule, at high temperature electron–phonon interaction dominates over electron–electron and electron–impurity scattering. Then, resistivity varies linearly with temperature. Resistivity of NAN6 is smaller than NAN2, NAN8, NAN9 and NAN10 films. The reasons for higher TCR and smaller resistively of NAN6 than other films are needed to be understood. For T<150K, several attempts have been made to fit the data to ρ = AT5, as dedicated by Matheissen's rule and also to Arrhenius expression, $\rho=\rho_0 exp(E/K_BT)$. But no good fits were achieved, implying that for these films, different theoretical treatment is required to understand resistivity below 150K.

3.2.3 Resistivity variation of NAN4 and NAN5 films

There is considerable amount of ρ(T) data on NAN4 and NAN5 films on either sides of the MST transition. Hence, temperature variation of resistivity of these two films has been separately analyzed. The negative temperature coefficient of resistance (TCR) below TC indicates localization of electrons and the positive TCR above TC suggests delocalization of electrons [27]. The delocalization of electrons leads to metallic conductivity, which is a characteristic feature of degenerate semiconductor [28]. The metal-semiconductor transition can be explained using a view proposed for conduction in disordered matter [29] where, the minima in the ρ(T) curve has been accounted for quantum correction (QC) terms in the conductivity expression. This view was developed based on Boltzmann semiclassical approach. The QC terms come from weak localization and Coulomb interaction effects that are related to structural disorder. The localization effects have already been considered to interpret the MST observed in various oxides such as RuO_2 [30], ZnO:Ga[27] and undoped ZnO thin films [31].

According to Lee and Ramakrishnan [29], the resistivity including the QC can be expressed as,

$$\rho=1/ (\sigma_o+a_1 T^{P/2} +a_2T^{1/2}) + (bT^2) \quad (4)$$

Here, $\rho_o(=1/\sigma_0)$ is the residual resistivity. The second term in the denominator corresponds to weak localization and the third term corresponds to Coulomb interaction effects. Eq. (4) was fit to the data of NAN4 and NAN5 as shown in Fig. 7. The best fit parameters obtained are recorded in Table 5. From the Table 5, it can be seen that in case of NAN4, $a_1>a_2$ and in the case of NAN5, $a_1<a_2$. These indicate that within QC, weak localization effect dominates over coulomb interaction in NAN4 film and reverse is the case in NAN5 film. The values of P for NAN4 and NAN5 were determined to be 0.5 and 1.8 respectively, which correspond to electron–phonon interaction at weak localization sites [28].

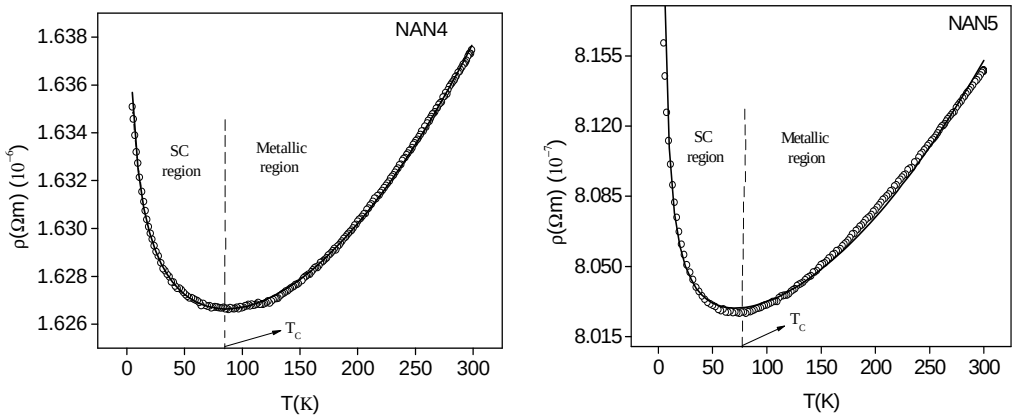

Fig. 7. ρ versus T for NAN4 and NAN5 films. Solid lines are the best fits to Eq. (4)

Table 5. Values of the fit parameters of Eq. (4) to the ρ(T) data on NAN4 and NAN5 films

Sample	σ_0 $(\Omega m)^{-1}$ x10^{-8}	a_1	P	a_2	B x10^{-6}
NAN4	1.14	33.5	0.5	1.62	0.167
NAN5	1.23	1.2	1.8	8.00	1.610

4. CONCLUSION

A set of sandwich films, Ni(100nm)/Al(t)/Ni(100nm); t =10nm to100nm were deposited by thermal and electron beam gun methods at 473 K under high vacuum conditions. The structure and grain sizes were probed through X-ray diffraction (XRD) studies. All the films exhibited (111) texture.

Low temperature electrical resistivity has been measured on all the films. Three films showed pure semiconducting behavior. The data of these films has been analyzed in the light of Mott's small polaron hopping model and variable range hopping models due to Mott and Greave.

Remaining seven films exhibited metal to semiconductor transition. Transition temperatures were determined. The data belonging to metallic region of these seven films obeyed Matheissen's rule of linear relation between resistivity and temperature. semiconducting tail was observed to be very short for five of the seven films. However, two of the films exhibited longer tails into metallic and semiconducting regions. The data of these two films has been fit to resistivity expression which incorporates quantum correction in to it. From this analysis, the coefficients corresponding to electron localization and coulomb interaction effects have been determined.

ACKNWLEDGEMENTS

Authors sincerely acknowledge the help received in the form of experimental facilities by Dr.V.Ganesan, Director, UGC-DAE Consortium for Scientific Research, Indore and other Scientists in the Centre Dr.Rajeev Rawat, Dr.N.P.Lalla, Dr.Mukul Gupta and Dr. V.Raghavendra Reddy.

COMPETING INTERESTS

Authors have declared that no competing interests exist.

REFERENCES

1. Kowalewski M, Heinrich B, Cochran JF, Schurer PJ. Studies of interlayer exchange coupling in Fe/Cu/Fe ultrathin heterostructures. Appl Phys.1997;8:3904-3906.
2. Jonson MT, Purcell ST, McGee NEW, Coehoorn R, aan de Stegge J, Hoving W. Structural dependence of the oscillatory exchange interaction across Cu layers. Phys Rev Lett. 1992,68:2688-2691.
3. Egelhoff Jr WF, Kief MT. Antiferromagnetic coupling in Fe/Cu/Fe and Co/Cu/Co multilayers on Cu(111). Phys Rev B condense Matter. 1992;45:7795-7804.

4. Heinrich B, Celinski Z, Cochran JF, Arrott AS, Mvrtle K. Bilinear and biquadratic exchange coupling in bcc Fe/Cu/Fe trilayers: Ferromagnetic-resonance and surface magneto-optical Kerr-effect studies. Phys. Rev. B. 1993;47:5077–5089.
5. Egelhoff Jr WF, Kef MT. Fe/Cu/Fe and Co/Cu/Co Multilayers on Cu (111): The absence of oscillatory antiferromagnetic coupling. IEEE Trans Magnetics; 1992;28:5.
6. Kumar Dileep, Gupta Ajay. Effects of interface roughness on interlayer coupling in Fe/Cr/Fe structure. Hyperfine Interactions. 2005;160:165-72.
7. Kholin DI, Drovosekov AB, Demokritov SO, Rickart M, Kreines NM. Noncollinear interlayer exchange in Fe/Cr/Fe magnetic structures with different interface roughness. Phys Metals Metallography. 2006;101:S67–S69.
8. Botana J, Pereiro M, Baldomir D, Kobayashi H, Arias JE.. Magnetic and electronic structure of nFe/3Cr/nFe slabs (n=1→6). Thin Solid Films. 2008;516:5144-5149.
9. Aliev FG, Moshchalkov VV, Bruynseraede Y. Anomalous low temperature of metallic trilayers-possible evidence for electron-scattering on symmetrical 2-level systems. Phys Rev. B. 1998;58:3625-3628.
10. Shamsutdinov NR, Bottger AJ, Tichelaar FD. The effect of Cu interlayers on grain size and stress in sputtered Fe-Cu multilayered thin films. Scripta Materialia. 2006;54: 1727-1732.
11. El Khiraouia S, Sajieddinea M, Hehnb M, Robertb S, Lenobleb O, Bellouardb C et al. Magnetic Studies of Fe/Cu Multilayers. Physica B. 2008;403:2509–2514.
12. Kumah DP, Cebollada A, Clavero C, Skuza JR, Lukaszew RA, Clarke R., Optimizing the planar structure of (1 1 1) Au/Co/Au trilayers. J Phys D Appl Phys. 2007;40: 2699–2704.
13. Sadashivaiah PJ, Sankarappa T, Sujatha T et al. Magnetic and Low Temperature Conducyivity Studies in Oxdised Nano Films J. Nano-Electron. Phys. 2011;3(4):43-54.
14. Manjunath AW, Sankarappa T, Ramanna R et al. Low temperature electrical resistivity studies in lead thin films. J. Nano-Electron. Phys. 2013;5:03026.
15. Sadashivaiah PJ, Sankrappa T, Sujatha T et al. Structural, magnetic and electrical properties of Fe/Cu/Fe. Vacuum. 2010;85:466-473.
16. Cullity of X-ray BD. Elements diffraction. Massachusetts, USA: Addison-Wesley Inc.; 1956.
17. Ravi Kumar, Abhinav Pratap Singh, Thakur P, Chae KH, Choi WK, Basavaraj nAngadi, Kaushik SD, Patnaik S. Ferromagnetism and metal-semiconducting transition in Fe-doped ZnO thin films. J. Phys D: Appl. Phys. 2008;41:1-5.
18. Bhosle V, Tiwari A, Narayan J. Metallic conductivity and metal-semiconductor transition in Ga-doped Zno, Appl. Phys. Lett. 88;032106-1-3.
19. Hakim A, Hossain J, Khan. Temperature effect on the electrical properties of undoped NiO thin films. Renew Energ. 2009;34;2625–2629.
20. Makhlouf SA. Electrical properties of Nio films obtained by high temperature oxidation of Nickel. Thin Solid Films. 2008;516:3112–3116.
21. Makhlouf SA, Kaseem MA, Rahim A. Particle size-dependent electrical properties of Nanocrystalline Nio. J. Matter. Sci. 2009;44:3438–3444.
22. Mott NF. Conduction in glasses containing transition metal ions. J. Non-Cryst. Solids 1968;1:1–17.
23. Mott NF. Conduction in non-crystalline materials. Phil. Mag. 1969;19:835-852.
24. Greaves GN. Small polaron conduction in V2O5P2O5 glasses. J. Non-Cryst. Solids 1973;11:427–446.
25. Elliot SR. Physics of amorphous materials (Longman London and New York; 1984.
26. El-Desoky MM. Small polaron transport in V2O5-NiO-TeO2 Glasses. J. Mater. Sci-Mater, Elect. 2003;14:215-221.

27. Pradhan AK, Douglas L, Mustata H, Mundle R, Hunter D, Bonner CE. Pulsed-laser deposited Er: ZnO films for 1.54 μm emission. Appl. Phys. Lett. 2007;90:072108.
28. Shimakawa K, Narushima S, Hosono H, Kawazoe H. Electronic transport in degenerate amorphous oxide semiconductors Philos. Mag. Lett. 1999;79(9):755 -761.
29. Lee PA, Ramakrishnan TV. Methods of quantum field theory in statistical physics. Rev. Mod. Phys. 1985;57:287.
30. Herranz G, Sanchez F, Martinez B, Fontcuberta J, Garcia-Cuenca MV, Ferrater C, Varela M, Levy P. Weak Localization effects in Some Metallic Pervoskites. Eur. Phys. J. B. 2004;40:439–444.
31. Nistor M, Gherendi F, Mandache NB, Hebert C, Perriere J, Seiler W. Metal-semiconductor transition in epitaxial ZnO thin films. J. Appl. Phys. 2009;106:103710.

Peer-review history:
The peer review history for this paper can be accessed here:
http://www.sciencedomain.org/review-history.php?iid=536&id=7&aid=5416